arXiv:1611.08111v1 [physics.space-ph] 24 Nov 2016

Revisiting a classic: the Parker-Moffatt problem

O. Pezzi[1], T.N. Parashar[2], S. Servidio[1], F. Valentini[1], C.L. Vásconez[3], Y. Yang[2], F. Malara[1], W.H. Matthaeus[2] and P. Veltri[1]

[1]Dipartimento di Fisica, Università della Calabria, 87036 Rende (CS), Italy.

[2]Department of Physics and Astronomy, University of Delaware, DE 19716, USA.

[3]Departamento de Física, Escuela Politécnica Nacional, Quito, Ecuador.

Received _____; accepted _____

ABSTRACT

The interaction of two colliding Alfvén wave packets is here described by means of magnetohydrodynamics (MHD) and hybrid kinetic numerical simulations. The MHD evolution revisits the theoretical insights described by Moffatt, Parker, Kraichnan, Chandrasekhar and Elsässer in which the oppositely propagating large amplitude wave packets interact for a finite time, initiating turbulence. However, the extension to include compressive and kinetic effects, while maintaining the gross characteristics of the simpler classic formulation, also reveals intriguing features which go beyond the pure MHD treatment.

Subject headings:

1. Introduction

A familiar perspective on the hydromagnetic description of astrophysical and laboratory plasma turbulence begins with the interaction of oppositely propagating large amplitude incompressible wave packets (Iroshnikov 1964; Kraichnan 1965). Various nonlinear phenomenologies are built on this paradigm (Dobrowolny et al. 1980a; Velli et al. 1989; Matthaeus et al. 1999; Galtier et al. 2000; Verdini et al. 2009; Ng & Bhattacharjee 1996). An essential feature is that large amplitude perturbations in which velocity $\mathbf{u}$ and magnetic field $\mathbf{b}$ fluctuations are Alfvénically correlated, i.e. either $\mathbf{u} = (c_A/B_0)\mathbf{b}$ or $\mathbf{u} = -(c_A/B_0)\mathbf{b}$ (where c_A and B_0 are uniform background Alfvén velocity and magnetic field, respectively), are exact stable solutions to the equations of incompressible magnetohydrodynamics (MHD) (Elsässer 1950; Chandrasekhar 1956). One thread emerging from this concerns the analysis of colliding wave packets to reveal properties of the MHD turbulence spectrum (Kraichnan 1965).

A different emphasis was given by Moffatt (1978) and Parker (1979). Both of these treatments analyzed the collision of large amplitude incompressible, ideal Alfvén wave packets noting that nonlinear interaction and mutual distortion of the wave packets are limited to the span of time during which they spatially overlap. Both *Moffatt* and *Parker* argued (somewhat differently, as discussed later) that the packets eventually separate and propagate once again undisturbed without further interactions. This paper addresses two questions that arise when trying to apply this physical insight to high temperature extraterrestrial plasmas such as the solar wind, where such large amplitude Alfvénic fluctuations are routinely observed (Belcher & Davis 1971), or solar corona, where the interaction of Alfvénic wave packets is thought to occur (Matthaeus et al. 1999). First, both compressibility effects and kinetic plasma are likely to be important in space applications, and we ask if these give rise to significant departures from the the Parker-Moffatt scenario.

Second, we ask whether the proposed separation of the packets after collision is realized as envisioned, or if a wake of non-propagating disturbances might remain after very long times. We address these specific questions using a compressible MHD model and a hybrid Vlasov model. Broader questions that emerge will be discussed in the concluding remarks.

In dealing with low Mach number quasi-incompressible fluid or MHD models, either in numerical simulations (Orszag 1971; Orszag & Patterson 1972; Kraichnan & Montgomery 1980), applications (Dobrowolny et al. 1980b; Matthaeus et al. 1999), or in analytical theory (Orszag 1977; Oughton et al. 2006), one routinely deals with two significant properties: first, the dominant quadratic couplings are of the form $\mathbf{k} = \mathbf{p} + \mathbf{q}$, transferring energy into (or from) Fourier mode with wave-vector $\mathbf{k}$ due to nonlinear interactions with modes at wave-vectors $\mathbf{p}$ and $\mathbf{q}$. One concludes that in general (unless, e.g., all excited wave vectors are co-linear) one expects excitations to spread rapidly among many wave-vectors, a process that over time can produce complex mixing and turbulent flows. Second, incompressible MHD nonlinear evolution proceeds as $\partial z_i^+/\partial t \sim -z_j^- \nabla_j z_i^+$ and $\partial z_i^-/\partial t \sim -z_j^+ \nabla_j z_i^-$ in terms of Elsässer variables $z_j^\pm = u_j \pm b_j$ (jth components of velocity field u_j and magnetic field b_j in Alfvén speed units), thus allowing the immediate conclusion that nonlinear couplings vanish unless the Elsässer fields $\mathbf{z}^+$ and $\mathbf{z}^-$ have nonzero overlap somewhere in space. These properties not only provide motivation for the Alfvén wave packet collision problem, but also enter into some of its complexity as an elementary interaction that generates turbulence (Kraichnan 1965; Dobrowolny et al. 1980b; Howes & Nielson 2013; Drake et al. 2016).

Beyond the assumption of incompressibility, we may anticipate genuinely compressible and kinetic effects that warrant examination in the large amplitude wave packets collision problem. In the solar wind for example, many intervals, especially within 1 AU (Bruno et al. 1985) or at high latitudes (McComas et al. 2000) are highly Alfvénic, but even

within such intervals there are mixtures of Elsässer amplitudes, small density variations, and a small parallel variance, as in the well-quoted "5:4:1" variance ratio reported by Belcher & Davis (1971). There have also been reports of interplanetary magneto-sonic wave packets interaction (He et al. 2015), while the great power-law in the interstellar medium (Armstrong et al. 1981) is associated with electron density fluctuations that may be either propagating or non-propagating (Zank & Matthaeus 1992). Furthermore in plasmas such as the solar wind, at smaller scales near the ion inertial scale, one expects kinetic properties (Alexandrova et al. 2008) such as spectral steepening (Bruno & Carbone 2013), dispersive wave effects (Sahraoui et al. 2007; Gary et al. 2010) of both Kinetic Alfvén Wave and whistler types, along with temperature anisotropy, beams and other distortions of the proton velocity distribution function (VDF) (Marsch 2006; Valentini et al. 2007; Servidio et al. 2012; Valentini et al. 2014; Servidio et al. 2015). These complications place the problem of collisions of Alfvén wave packets in a much more complex framework.

2. Models and Approach

Motivated by these considerations, we revisit the problem of two colliding large amplitude Alfvén wave packets by means of compressible fluid and kinetic Vlasov-Maxwell simulations. The shown results are from a magnetohydrodynamics (MHD) model and a hybrid kinetic plasma (HVM) model. Both retain 2.5 dimensions in the physical space, with three Cartesian fluid velocities and field components, but with gradients only in the (x, y) plane. The HVM model has also a three dimensional velocity space grid.

It is clear that this problem would be better addressed in a high resolution fully 3D representation in physical space. However, computational cost limits accessible 3D simulations to relatively low spatial resolution. This present geometry is favored because it allows for a large system size, that, in turn, ensures a large Reynolds number and hence

MHD like turbulent dynamics (Parashar et al. 2015a), as well as a realistic realization of compressive fluctuations/parallel variances (Parashar et al. 2016).

The dimensionless MHD equations are:

$$\partial_t \rho + \nabla \cdot (\rho \mathbf{u}) = 0 \tag{1}$$

$$\partial_t \mathbf{u} + (\mathbf{u} \cdot \nabla)\mathbf{u} = -\frac{\tilde{\beta}}{2\rho}\nabla(\rho T) + \frac{1}{\rho}\left[(\nabla \times \mathbf{B}) \times \mathbf{B}\right] \tag{2}$$

$$\partial_t \mathbf{B} = \nabla \times (\mathbf{u} \times \mathbf{B}) \tag{3}$$

$$\partial_t T + (\mathbf{u} \cdot \nabla)T + (\gamma - 1)T(\nabla \cdot \mathbf{u}) = 0 \tag{4}$$

In Eqs. (1)–(4) spatial coordinates $\mathbf{x} = (x, y)$ and time t are respectively normalized to $\tilde{L}$ and $\tilde{t}_A = \tilde{L}/\tilde{c}_A$. The magnetic field $\mathbf{B} = \mathbf{B}_0 + \mathbf{b}$ is scaled to the typical magnetic field $\tilde{B}$, while mass density ρ, fluid velocity $\mathbf{u}$, temperature T and pressure $p = \rho T$ are scaled to typical values $\tilde{\rho}$, $\tilde{c}_A = \tilde{B}/(4\pi\tilde{\rho})^{1/2}$, $\tilde{T}$ and $\tilde{p} = 2\kappa_B\tilde{\rho}\tilde{T}/m_p$ (being κ_B the Boltzmann constant and m_p the proton mass), respectively. Moreover, $\tilde{\beta} = \tilde{p}/(\tilde{B}^2/8\pi)$ is a typical value for the kinetic to magnetic pressure ratio; $\gamma = 5/3$ is the adiabatic index. Details about the numerical algorithm can be found in Vásconez et al. (2015); Pucci et al. (2016).

The kinetic simulations solve the hybrid Vlasov-Maxwell equations system (Valentini et al. 2007) in which the proton distribution function is numerically evolved while electrons are a massless Maxwellian, isothermal fluid. Dimensionless HVM equations are:

$$\partial_t f + \mathbf{v} \cdot \nabla f + \frac{1}{\tilde{\epsilon}}(\mathbf{E} + \mathbf{v} \times \mathbf{B}) \cdot \nabla_{\mathbf{v}} f = 0 \tag{5}$$

$$\mathbf{E} = -\mathbf{u} \times \mathbf{B} + \frac{\tilde{\epsilon}}{n}\left(\mathbf{j} \times \mathbf{B} - \frac{\tilde{\beta}}{2}\nabla P_e\right) \tag{6}$$

$$\frac{\partial \mathbf{B}}{\partial t} = -\nabla \times \mathbf{E} \quad ; \quad \nabla \times \mathbf{B} = \mathbf{j} \tag{7}$$

where $f = f(\mathbf{x}, \mathbf{v}, t)$ is the proton distribution function. In Eqs. (5)–(7), velocities $\mathbf{v}$ are scaled to the Alfvén speed $\tilde{c}_A$, while the proton number density $n = \int f\, d^3v$ and the proton bulk velocity $\mathbf{u} = n^{-1}\int \mathbf{v} f\, d^3v$, obtained as moments of the distribution function,

are normalized to $\tilde{n} = \tilde{\rho}/m_p$ and $\tilde{c}_A$, respectively. The electric field $\mathbf{E}$, the current density $\mathbf{j} = \nabla \times \mathbf{B}$ and the electron pressure P_e are scaled to $\tilde{E} = (\tilde{c}_A \tilde{B})/c$, $\tilde{j} = c\tilde{B}/(4\pi \tilde{d}_p)$ and $\tilde{p}$, respectively. Finally, the parameter $\tilde{\epsilon} = \tilde{d}_p/\tilde{L}$, where $\tilde{d}_p = \tilde{c}_A/\tilde{\Omega}_{cp}$ is the proton skin depth, allows a comparison of fluid and kinetic scales. Electron inertia effects have been neglected in the Ohm's law and no external resistivity η is introduced. A detailed description of the HVM algorithm can be found in Valentini et al. (2007); Vásconez et al. (2015); Servidio et al. (2015).

The simulations are set up as follows. The spatial domain $D(x, y) = [0, 8\pi] \times [0, 2\pi]$ has been discretized with $(N_x, N_y) = (1024, 256)$ mesh points, thus implying $\Delta x = \Delta y$ and also an anisotropic wave-vectors space. Spatial boundary conditions are periodic. In the HVM run, we adopted a uniform velocity space grid with 51 points in each direction, in the region $v_i = [-v_{max}, v_{max}]$, being $v_{max} = 2.5\tilde{c}_A$. Velocity domain boundary conditions assume $f = 0$ for $|v_i| > v_{max}$ $(i = x, y, z)$. In our simulation we set $\beta_p = 2v_{th,p}^2/\tilde{c}_A^2 = \tilde{\beta}/2 = 0.5$, which corresponds to $v_{max} = 5v_{th,p}$, and $\tilde{\epsilon} = 9.8 \times 10^{-2}$. The background magnetic field is mainly perpendicular to the $x - y$ plane, indeed $\mathbf{B_0} = B_0(\sin\vartheta, 0, \cos\vartheta)$, being $\vartheta = \cos^{-1}\left[(\mathbf{B_0} \cdot \hat{\mathbf{z}})\,/B_0\right] = 6^\circ$ and $B_0 = |\mathbf{B_0}|$.

We impose large amplitude magnetic $\mathbf{b}$ and bulk velocity $\mathbf{u}$ perturbations. Density perturbations are not imposed, which implies nonzero total pressure fluctuations. In the HVM case, the proton VDF is initially Maxwellian at each spatial point. Initial perturbations consist of two Alfvénic wave packets with opposite velocity-magnetic field correlation, separated along x. Because $B_{0,x} \neq 0$, the packets counter-propagate. The nominal time for the collision, which has been evaluated from the center of each wave packet, is about $\tau \simeq 58.9$.

The magnetic field perturbation $\mathbf{b}$ has been created by initializing energy in the first four wave-numbers in the y direction while, due to the x spatial localization (enforced

by projection), many wave-numbers along x are excited initially. Then, a small $b_z(x, y)$ component has been introduced in such a way that the transverse condition, $\mathbf{B_0} \cdot \mathbf{b} = 0$, is hold in each domain point. Finally, the velocity field perturbation $\mathbf{u}$ is generated by imposing that $\mathbf{u}$ and $\mathbf{b}$ are correlated (anti-correlated) for the wave packet which moves against (along) the magnetic field B_{0x}. The intensity of the perturbation is $\langle b \rangle_{rms}/B_0 = 0.2$, therefore the Mach number is $M_s = \langle u \rangle_{rms}/v_{th,p} = 0.4$. The intensity of fluctuations with respect to the in-plane field B_{0x} is quite strong, with a value of about 2. It is worth to note that the inverse of the intensity of the fluctuations with respect to the in-plane magnetic field is related to the parameter τ_{NL}/τ_{coll}, where τ_{NL} is the characteristic nonlinear time and τ_{coll} is the characteristic collision time. If $\tau_{NL}/\tau_{coll} \lesssim 1$, several nonlinear times occur in a single collision and wave packets can be significantly perturbed by nonlinear effects. On the other hand, if $\tau_{NL}/\tau_{coll} > 1$, many collisions are necessary to strongly distort wave packets. By evaluating $\tau_{NL} \simeq \Delta/u$ (wave packet width Δ, perturbations amplitude u) and $\tau_{coll} \simeq \Delta/V$ (in-plane Alfvén propagation speed $V \simeq 0.1 c_A$), it turns out that $\tau_{NL}/\tau_{coll} \simeq 0.5$. Therefore our simulations stand in a parameter range where nonlinear effects can be such important that a strong turbulence scenario may be present.

2.1. Discussion of the Initial Conditions

The imposed initial perturbations correspond to two large amplitude Alfvén wave packets in the sense that magnetic and velocity perturbations are fully correlated in each packet, and the packets are separated in space. With zero density variation, a weak in-plane uniform magnetic field, and a relatively strong out of plane uniform magnetic field, this initial condition is one for which the reasoning of Moffatt and Parker discussed above would be applicable in the context of an incompressible model.

In addition, the initial data also exactly satisfy the transversality condition $\mathbf{B_0} \cdot \mathbf{b} = 0$,

which in linear compressible MHD would correspond to the Alfvén eigenmode, if indeed the amplitude were infinitesimal. Here the amplitude is large, so small amplitude theory is unlikely to be relevant to the nonlinear evolution. Furthermore, the condition of the proper Alfvén eigenmode obtained in large amplitude compressible MHD theory, namely $B = |\mathbf{B}| = const$ is not satisfied by our initial perturbations (Barnes 1979). This suggests that pressure and density fluctuations may be generated during the wave packets evolution. Therefore the initial data are nonlinear eigenmodes of incompressible MHD, but not exact eigenmodes of compressible MHD. On the other hand we do not expect significant differences because the initial $B = |\mathbf{B}|$ fluctuations are not very large (less than 10%). Future works will analyze the evolution in the case in which $B = const$ at $t = 0$, and in the framework of other plasma models, such as Hall MHD and Particle In Cell (PIC) kinetic plasma models.

3. Numerical Results

An overview of the dynamics in the two simulations (MHD and HVM) can be appreciated by inspection of the evolution of the out-of-plane component of the current density $j_z(x, y)$, reported in Fig. 1. Left and right columns of Fig. 1 refer to the MHD and HVM simulations, respectively. The rows refer to different instants of time: top, center and bottom rows respectively indicate $t = 29.4$, $t = \tau = 58.9$ and $t = 88.4$. In both simulations the initially separated wave packets counter-propagate, approach each other [top panels of Fig. 1], and collide at $t = \tau$. During the collision [center panels of Fig. 1], j_z intensifies, and, since the overlapping wave packets interact nonlinearly, the dynamics produces small scales that can be easily appreciated by examining the width of the current structures in the center row of Fig. 1. At the final stages of the simulations [bottom panels of Fig. 1], the wave packets continue their motion while displaying a significantly perturbed shape.

Indeed the j_z contours indicate that current structures are much more complex after that the collision occurs. Moreover, their shape exhibits also a curvature which is not anticipated prior to the collision and which indicates the presence of energy in modes with gradients along the y direction, transverse to the propagation.

The MHD and HVM evolutions exhibit noticeable differences: the MHD case is symmetric with respect to $x = L_x/2 \approx 12.5$, while this symmetry is lost in the Vlasov run also before the collision [right top panel of Fig. 1]. The lack of the symmetry in the HVM run may be due to the inter-coupling of B_{0x} and dispersive effects which are present in the HVM run and may cause a different propagation along and against B_{0x}. The HVM run also forms smaller scales during the interaction than in the MHD case. This difference can be appreciated in the right, center panel of Fig. 1. Finally, after the collision, j_z is much more complex in the HVM simulation than in the MHD run. Very thin current sheet structures and secondary ripples are observed only in the Vlasov case. The nature of these secondary ripples may be associated with the presence of some KAW-like fluctuations (Hollweg 1999; Vásconez et al. 2015) and will be analyzed in detail in a separate paper.

A point of comparison of our simulations with respect to the theoretical ideas given by Moffatt and Parker is to examine the behavior of cross helicity. Those theoretical treatments assume ideal non-dissipative conditions, so that the total cross helicity is conserved and moreover the expectation is that the separate wave packets after the collision have the same cross helicity as prior to the interaction. Furthermore the initial and final states, in the ideal treatment, have equipartition of flow and magnetic field energy, with departures from equipartition possible during the interaction. To examine these, Fig. 2 shows the temporal evolution of (a) the normalized cross-helicity $\sigma_c(t)$, and (b) the normalized residual energy $\sigma_r(t)$ (Bruno & Carbone 2013), respectively defined as $\sigma_c = (e^+ - e^-)/(e^+ + e^-)$ and $\sigma_r = (e^u - e^b)/(e^u + e^b)$, where $e^\pm = \langle(\mathbf{z}^\pm)^2\rangle/2$, $e^u = \langle\mathbf{u}^2\rangle/2$, $e^b = \langle\mathbf{b}^2\rangle/2$ and $\mathbf{z}^\pm = \mathbf{u} \pm \mathbf{b}$.

The normalized cross-helicity $\sigma_c(t)$ is well-preserved in the MHD simulation, while, in the kinetic simulation, $\sigma_c(t)$ displays, around the collision time τ, a significant growth followed by a saturation stage. It is worth to note that, in the MHD run, $\sigma_c(t)$ is still conserved despite $\sigma_c(t)$ is an invariant of the incompressible MHD while our MHD simulation is compressible [compressibility could, in principle, break the invariance of $\sigma_c(t)$]. This characteristic reflects the fact that the compressive fluctuations which are dynamically generated during the MHD evolution are not strong enough to break the invariance of $\sigma_c(t)$. On the other hand, the breaking of the σ_c invariance in the Vlasov run is associated with the presence of both dispersive and kinetic effects. Indeed, by evaluating the incompressible Hall MHD invariant σ_g (generalized helicity) (Turner 1986; Servidio et al. 2008), σ_g is also not preserved for the HVM run and it shows a similar behavior of σ_c (in particular a jump is recovered at $t \simeq \tau$). This feature suggests that the production of $\sigma_c(t)$ recovered in the kinetic simulation cannot be associated only with dispersive effects, which are taken into account in the Hall model, but is also due to the presence of kinetic effects.

In contrast the evolution of the residual energy $\sigma_r(t)$ is very similar in the MHD and HVM simulations. Referring to Fig. 2 (b), we see that in the initial stages $\sigma_r \simeq 0$, then σ_r strongly oscillates during the wave packets collisions, first to positive values indicating a positive correlation of the Elsässer fields, then moving more strongly towards negative values of correlation, and returning to positive correlation again prior to finally approaching zero once again. It is clear that during the collision there is substantial exchange of kinetic and magnetic energy, and this is not greatly influenced by kinetic effects.

In order to compare the role of small scale dynamics in the two cases, we computed the mean square out-of-plane electric current density $\langle j_z^2 \rangle$ as a function of time. This is illustrated in the top panel of Figure 3 for the MHD (black) and kinetic HVM (red) runs. In both cases, $\langle j_z^2 \rangle(t)$ shows a similar time evolution. In particular, both models show a peak of

$\langle j_z^2 \rangle(t)$ around the collision time $t \simeq \tau$. After the collision, a high-intensity current activity persists and the peak of current activity is reached in the final stage of the simulations.

Other quantities that provide further physical details about the simulations are $\langle \delta\rho^2 \rangle$, the density fluctuations providing a measure of compressibility, and $\langle \omega^2/2 \rangle$, the mean square vorticity or enstrophy, where $\delta\rho = \rho - \langle \rho \rangle$ and $\omega = \nabla \times \mathbf{u}$. Panels (b) and (c) of Figure 3 respectively show $\langle \delta\rho^2 \rangle$ and $\langle \omega^2/2 \rangle$ for both simulations. The density fluctuations peak around $t \simeq 65$ and $t \simeq 85$. The first peak is due to the interaction between the two wave packets. The second peak of density fluctuations appears to be due to propagation of magneto-sonic fluctuations generated by the initial strong collision. Once generated these modes propagate across the periodic box and provide an "echo" of the original collision. We also note that in the initial stage of both simulations, $\langle \delta\rho^2 \rangle$ exhibits some small modulations, which could be produced by the absence of a pressure balance in the initial condition.

The enstrophy $\langle \omega^2/2 \rangle$ evolution, also shown in Fig. 3, indicates that both MHD and HVM cases produce fine scale structure in the velocity, i.e., vortical structures, during the collisions, and these persist after the collision. However, in the MHD case $\langle \omega^2/2 \rangle$ reaches larger values compared to the HVM case. This could be due to the presence of kinetic damping effects which decrease the intensity of $\langle \omega^2/2 \rangle$ by transferring energy to the VDF [see. e.g., Del Sarto et al. (2016); Parashar & Matthaeus (2016)]. It is interesting to note that the general profile of enstrophy and mean square current follow similar trends in time. This can be expected as the inertial range of turbulence typically provides near-equipartition of velocity and magnetic fluctuation energy, even in fairly simple configurations (Matthaeus & Lamkin 1986). However, when examined in more detail, one often finds, as here, that the magnetic fluctuations are usually about a factor of two more energetic in the inertial range part of the spectrum, as they are, for example in the solar

wind (Matthaeus & Goldstein 1982). This inequality is here reflected in the fact that $\langle j_z^2 \rangle > \langle \omega^2/2 \rangle$.

In order to further characterize the small scales fluctuation generated by the collisions and associated nonlinear activity, we examine the magnetic energy spectra. Figs. 4 shows, for the Vlasov run, the reduced magnetic field power spectral densities $E_{b,y}(k_x)$ (black) and $E_{b,x}(k_y)$ (red) at (a) $t = 29.4$; (b) $t = \tau = 58.9$; and (c) $t = 88.4$. Here, for example, $E_{b,y}(k_x)$ is a one-dimensional reduced power spectra density obtained by integrating over one component of wave-vector. The blue dashed lines in Fig. 4 indicate a $k^{-5/3}$ slope for reference. We remark that the spectra for the HVM run show more energy at very small scales compared to the MHD run (not shown here), again consistent with the idea that the HVM run produces more fine scales than the the MHD simulation. This may simply indicate that the effective dissipation in the HVM case is smaller than the numerically motivated dissipation coefficients selected for the MHD run.

In Fig. 4 we observe that, at $t = 29.4$, the spectrum $E_{b,y}(k_x)$ is steep due to the localization of the initial condition, which requires involvement of a wide range of wave-numbers k_x. Furthermore, during the evolution, the spectra show a transfer of energy towards small scales, at higher k_x and at higher k_y. This represents a signature of energy transfer due to nonlinear coupling. In fact, much of the energy $E_{b,y}(k_x)$ is contained, at $t = \tau$, in a bump around $k = 1$, while at $t = 88.4$ the bump is less clear and the spectrum $E_{b,y}(k_x)$ is more developed compared to the one at $t = \tau$. A break in $E_{b,y}(k_x)$ can be also appreciated around $k_{d_p} \simeq 10$.

Another feature of the magnetic energy spectra is that $E_{b,x}(k_y)$, which initially contains less energy than $E_{b,y}(k_x)$, experiences a significant increase in power, reaching almost the same amplitude at the later times. This suggests that fluctuations become more isotropic, and that energy transfer is efficient in both directions of the wave-vector space.

4. Conclusions

We have carried out a comparative study using different plasma simulation methods to examine the dynamical evolution that accompanies the interaction or collision of two oppositely propagating wave packets. For the classic case of incompressible MHD, considered by Moffatt and by Parker, the wave packets are, when considered separately, exact large amplitude solutions of the nonlinear equations, and are, therefore, strictly speaking "waves". If two such waves, oppositely propagating, become overlapping, nonlinear couplings and turbulence can be produced and the packets are deformed. Moffatt and Parker concluded that, after the characteristic interaction time, the packets again separate and continue propagating away from one another without further nonlinear interactions. Hence one question addressed in the present study is whether such separation after a collision actually occurs. A second question is whether departures from incompressible MHD change the dynamics in an appreciable way. To that end, here we examined a compressible MHD formulation and a hybrid Vlasov formulation.

Our results show that - when one moves beyond the MHD framework in which the Moffatt & Parker problem is approached - the dynamics become more complex. Here we find that, in both the present cases, the interactions and the structures produced in the collision are sufficiently complex that it is difficult to determine whether the wave packets actually attain a full separation after the collision. Indeed, we note that very complex current and vorticity structures are produced at small scales in both compressible MHD and HVM cases and these fluctuations are indicative of a spread of energy in the wave vectors plane, which is almost perpendicular to $\mathbf{B_0}$. The energy spectra evolve toward isotropy in this plane, although one would expect a degree of spectral anisotropy to persist due to the presence of the weak in-plane magnetic field. Furthermore, to the extent that the interaction of the packets has a finite lifetime [as envisioned e.g. by Kraichnan (1965)],

any such relaxation would be expected to be incomplete in a single interaction time.

In addition, we recall that in the incompressible ideal problem, cross helicity is conserved, so that after the collision in that case, the separated wave packets will each contain the same energy that was present in the initial state. However, cross-helicity is not preserved in the kinetic case since dispersive (e.g. Hall effect) and dissipative effects are present in the simulation. In fact in the HVM case, we observe a significant change in global cross helicity during the interaction.

This preliminary examination of the fate of the Moffatt and Parker conjecture in the context of compressible as well as kinetic models has produced a satisfactory, if not complete, picture. In fact the basic physics of the large amplitude Alfvén waves collisions as envisioned by those authors appears to be upheld in this regime. However, we have neither examined the most general case, which would require full 3D simulations nor have we completely analyzed the compressible and kinetic effects in the present cases. In particular, not shown here are indications of specific kinetic wave modes and characteristic distortions of the velocity distribution function (Servidio et al. 2015; Vásconez et al. 2015) that might be expected. A separate account of these results is in preparation. We also note that we have analyzed the present problem employing several other models including hybrid particle in cell, Hall MHD and also varying the initial conditions. Such results are of interest in the context of e.g. Turbulent Dissipation Challenge (Parashar et al. 2015b) and will be reported at a later time.

Research is supported by NSF AGS-1063439, AGS-1156094 (SHINE), AGS-1460130 (SHINE), and NASA grants NNX14AI63G (Heliophysics Grandchallenge Theory), and the Solar Probe Plus science team (ISIS/SWRI subcontract No. D99031L), and Agenzia Spaziale Italiana under the contract ASI-INAF 2015-039-R.O “Missione M4 di ESA: Partecipazione Italiana alla fase di assessment della missione THOR”. Kinetic numerical

simulations here discussed have been run on the Fermi supercomputer at Cineca (Bologna, Italy), within the ISCRA-C project IsC37-COLALFWP (HP10CWCE72).

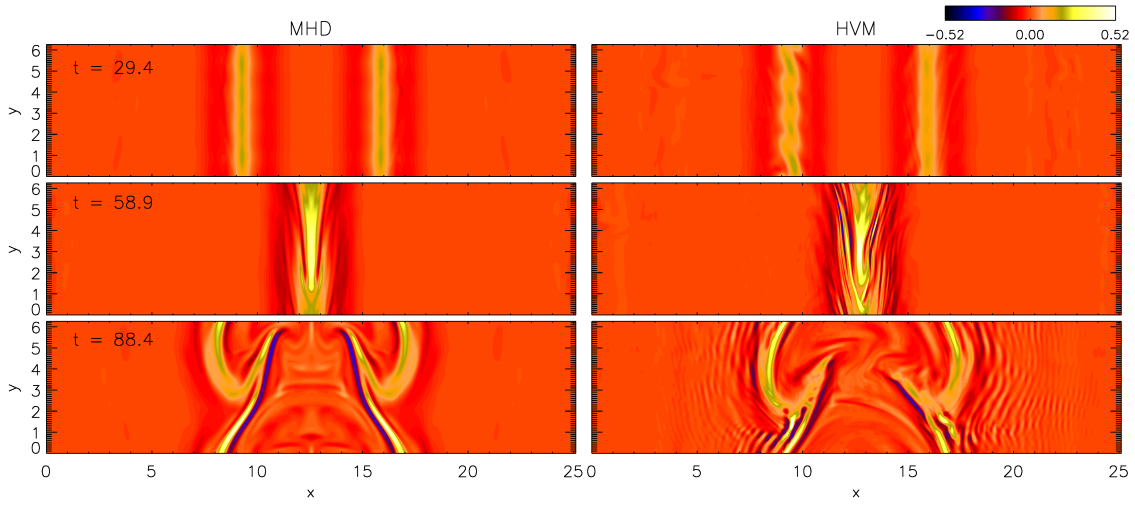

Fig. 1.— (Color online) Contour plots of the current density $j_z(x, y)$ for the MHD (left column panels) and the HVM (right column panels) simulations. Top, center and bottom rows correspond respectively to the time instants $t = 29.4$, $t = \tau = 58.9$ and $t = 88.4$.

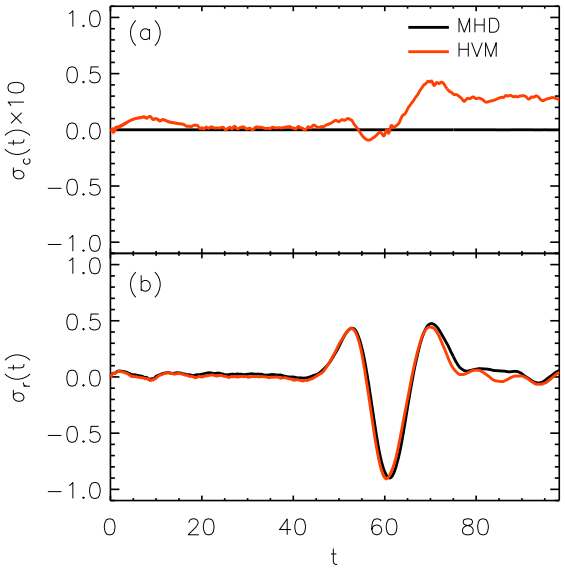

Fig. 2.— (Color online) Temporal evolution of $\sigma_c(t)$ (a) and $\sigma_r(t)$ (b). In each panel black and red lines refer to the MHD and HVM cases, respectively.

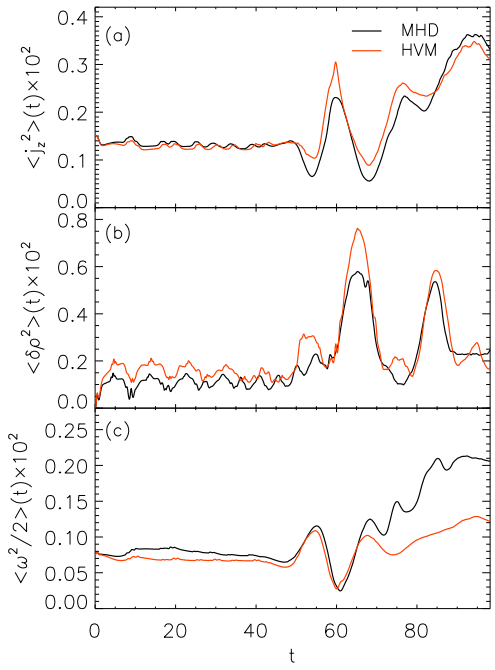

Fig. 3.— (Color online) Temporal evolution of $\langle j_z^2\rangle(t)$ (a), and $\langle\delta\rho^2\rangle(t)$ (b) and $\langle\omega^2/2\rangle(t)$ (c) for the MHD (black line) and HVM (red line) simulations.

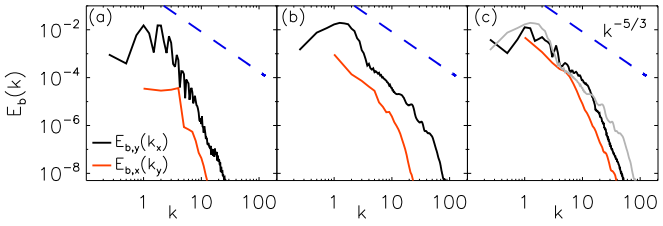

Fig. 4.— (Color online) Power spectra density of the magnetic energy E_b at three time instants $t = 29.4$ (a), $t = \tau = 58.9$ (b) and $t = 88.4$ (c). In each panel the black curve indicates $E_{b,y}(k_x) = \langle E_b(k_x, k_y)\rangle_{k_y}$, the red curve refers to $E_{b,x}(k_y) = \langle E_b(k_x, k_y)\rangle_{k_x}$ and the dashed blue line indicates the slope $k^{-5/3}$ as a reference. The gray line in panel (c) represents $E_{b,y}(k_x)$ at $t = 58.9$, which corresponds to the black line of panel (b).

REFERENCES

Alexandrova, O., Carbone, V., Veltri, P., & Sorriso-Valvo, L. 2008, ApJ, 674, 1153

Armstrong, J., Cordes, J., & Rickett, B. 1981, Nature, 291, 561

Barnes, A. 1979, Space Plasma Physics: The Study of Solar-System Plasmas (National Academy of Sciences, Washington, DC USA)

Belcher, J.W., & Davis Jr., L. 1971, J. Geophys. Res., 76, 3534

Bruno, R., Bavassano, R., & Villante, U. 1985, J. Geophys. Res., 90, 4373

Bruno, R., & Carbone, V. 2013, Living Reviews Solar Physics, 10, 1

Chandrasekhar, S. 1956, Proceedings of the National Academy of Sciences, 42, 273

Del Sarto, D., Pegoraro, F., & Califano, F. 2016, Phys. Rev. E , 93, 053203

Dobrowolny, M., Mangeney, A., & Veltri, P. 1980, Phys. Rev. Lett., 45, 144

Dobrowolny, M., Mangeney, A., & Veltri, P. 1980, Solar and Interplanetary Dynamics (Springer, Netherlands).

Drake, D.J., Howes, G.G., Rhudy, J.D., Terry, S.K., Carter, T.A., Kletzing, C.A., Schroeder, J.W.R., & Skiff, F. 2016, Phys. Plasmas, 23, 022305

Elsässer, W.M. 1950, Phys. Rev., 79, 183

Galtier, S., Nazarenko, S.V., Newell, A.C., & Poucket, A. 2000, J. Plasma Phys., 63, 447

Gary, S.P., Saito, S., & Narita, Y. 2010, ApJ, 716, 1332

He, J., Tu, C., Marsch, E., Chen, C.H.K., Wang, L., Pei, Z., Zhang, L., Salem C.S., & Bale, S.D. 2015, ApJ, 813, L30

Hollweg, J.V. 1999, J. Geophys. Res., 104, 14811

Howes, G.G., & Nielson, K.D. 2013, Phys. Plasmas, 20, 072302

Iroshnikov, R.S. 1964, Soviet Astron., 7, 566

Kraichnan, R.H. 1965, Phys. Fluids, 8, 1385

Kraichnan, R.H., & Montgomery, D. 1980, Reports on Progress in Physics, 43, 547

Marsch, E. 2006, Living Rev. Sol. Phys., 3, 1

Matthaeus, W.H., & Goldstein, M.L. 1982, J. Geophys. Res., 87, 6011

Matthaeus, W.H., & Lamkin, S.L. 1986, Phys. Fluids, 29, 2513

Matthaeus, W.H., Zank, G.P., Oughton, S., Mullan, D.J., & Dmitruk, P. 1999, ApJ, 523, L93

Matthaeus, W.H., Zank, G.P., Smith, C.W., & Oughton, S. 1999, Phys. Rev. Lett., 82, 3444

McComas, D.J., Barraclough, L., Funsten, H.O., Gosling, J.T., Santiago-Muñoz, E., Skoug, R.M., Goldstein, B.E., Neugebauer, M., Riley, P., & Balogh, A. 2000, J. Geophys. Res., 105, 419

Moffatt, H.K. 1978, Field Generation in Electrically Conducting Fluids (Cambridge University Press)

Ng, C.S., & Bhattacharjee, A. 1996, ApJ, 465, 845

Orszag, S. 1971, Stud. Appl Math., 50, 293

Orszag, S.A., & Patterson, G.S. 1972, Phys. Rev. Lett., 28, 76

Orszag, S.A. 1977, in Fluid Dynamics: Les Houches 1973, ed. by R. Balian and J. L. Peube (Gordon and Breach, New York), 237

Oughton, S., Dmitruk, P., & Matthaeus, W.H. 2006, Phys. Plasmas, 13, 2306

Parashar, T.N., Matthaeus W.H., Shay, M.A., & Wan, M. 2015, ApJ, 811, 112

Parashar, T.N., Salem, C., Wicks, R.T., Karimabadi, H., Gary, S.P., & Matthaeus, W.H. 2015, J. Plasma Phys., 81, 905810513

Parashar, T.N., Oughton, S., Matthaeus W.H., & Wan, M. 2016, ApJ, 824, 44

Parashar, T.N. & Matthaeus W.H. 2016, ApJ, submitted

Parker, E.N. 1979, Cosmical magnetic fields: Their origin and their activity (Oxford University Press)

Pucci, F., Vásconez, C.L., Pezzi, O., Servidio, S., Valentini, F., Matthaeus, W.H., & Malara, F. 2016, J. Geophys. Res., 121, 1024

Sahraoui, F., Galtier, S., & Belmont, G. 2007, J. Plasma Phys., 73, 723

Servidio, S., Matthaeus, W.H., & Carbone, V. 2008, Phys. Plasmas, 15, 042314

Servidio, S., Valentini, F., Califano, F., & Veltri, P. 2012, Phys. Rev. Lett., 108, 045001

Servidio, S., Valentini, F., Perrone, D., Greco, A., Califano, F., Matthaeus W.H., & Veltri, P. 2015, J. Plasma Phys., 81, 325810107

Turner, L. 1986, IEEE Transactions on Plasma Science, 14, 849

Valentini, F., Travnicek, P., Califano, F., Hellinger, P., & Mangeney, A. 2007, J. Comput. Phys., 225, 753

Valentini F., Servidio S., Perrone D., Califano F., Matthaeus W. H., & Veltri, P. 2014, Physics of Plasmas, 21, 082307

Vásconez, C.L., Pucci, F., Valentini, F., Servidio, S., Matthaeus, W.H., & Malara, F. 2015, ApJ, 815, 7

Velli, M., Grappin, R., & Mangeney, A. 1989, Phys. Rev. Lett., 63, 1807

Verdini, A., Velli, M., & Buchlin, E. 2009, The Astrophys. Journal Letters, 700, L39

Zank, G.P., & Matthaeus, W.H. 1992, J. Geophys. Res., 97, 189

This manuscript was prepared with the AAS LaTeX macros v5.2.